Editors' Suggestion | Featured in Physics

Telecom-Wavelength Quantum Repeater Node Based on a Trapped-Ion Processor

V. Krutyanskiy,[1,2] M. Canteri,[2,1] M. Meraner,[2,1] J. Bate,[1] V. Krcmarsky,[2,1]
J. Schupp,[2,1] N. Sangouard,[3] and B. P. Lanyon[1,2,*]

[1]*Institut für Experimentalphysik, Universität Innsbruck, Technikerstrasse 25, 6020 Innsbruck, Austria*
[2]*Institut für Quantenoptik und Quanteninformation, Osterreichische Akademie der Wissenschaften, Technikerstrasse 21a, 6020 Innsbruck, Austria*
[3]*Institut de Physique Théorique, Université Paris-Saclay, CEA, CNRS, 91191 Gif-sur-Yvette, France*

(Received 19 October 2022; revised 17 February 2023; accepted 16 March 2023; published 22 May 2023)

A quantum repeater node is presented based on trapped ions that act as single-photon emitters, quantum memories, and an elementary quantum processor. The node's ability to establish entanglement across two 25-km-long optical fibers independently, then to swap that entanglement efficiently to extend it over both fibers, is demonstrated. The resultant entanglement is established between telecom-wavelength photons at either end of the 50 km channel. Finally, the system improvements to allow for repeater-node chains to establish stored entanglement over 800 km at hertz rates are calculated, revealing a near-term path to distributed networks of entangled sensors, atomic clocks, and quantum processors.

DOI: 10.1103/PhysRevLett.130.213601

Envisioned quantum networks consist of distributed matter-based nodes, for quantum information processing and storage, that are interconnected with quantum channels for photons to establish internode entanglement [1,2]. Such networks would enable a range of new applications [2] and are desirable over distances that span a single lab up to those required for a global quantum internet. The bottleneck for implementing quantum networks over long distances—the exponentially increasing probabilities of losing photons or having their information scrambled with the channel length—could be overcome by building *quantum repeaters* [3–10]. With quantum repeaters, the distance between entangled end nodes in quantum network demonstrations [11–24] could be scaled up far beyond the attenuation length of the best photonic waveguides: optical fibers for telecom wavelengths.

Following the original scheme [3], quantum repeater nodes (Fig. 1) for fiber-based networks require a combination of capabilities including (1) interfaces between stationary qubit registers and telecom photons and (2) quantum memories with storage times longer than the remote entanglement generation time. Significant progress has been made toward developing these capabilities using ensemble-based memories [5], including with telecom interfaces [25–27]. Memory-enhanced communication has been achieved over short distances with individual [28] and ensembles [29,30] of atoms, and with solid-state vacancy centers [31,32]. However, there are significant advantages if repeater nodes have a third capability: (3) deterministic quantum information processing [33]. Without telecom-wavelength interfaces, capabilities (1)–(3) were combined in systems of vacancy centers a few meters apart and used for entanglement distillation [34], teleportation [35], and entanglement of three nodes [15]. Open challenges are to combine all the above capabilities in a single system and use them to demonstrate repeater-assisted entanglement distribution over tens of kilometers: internode distances over which repeaters could offer significant advantages for entangling matter, over repeaterless schemes. Because of the extended photon travel times and lower success probabilities, achieving repeater-assisted entanglement distribution over tens of kilometers places far stronger demands on system performance than over a few meters.

In this Letter, a repeater node based on trapped ions is first presented that combines capabilities (1)–(3), as envisioned in Ref. [33], and used to demonstrate repeater-assisted entanglement distribution over a 50 km channel.

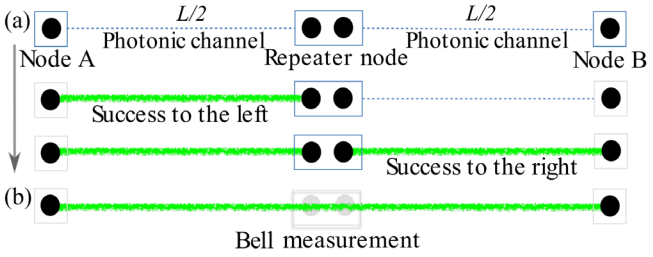

FIG. 1. Quantum repeater concept. (a) A repeater node attempts to establish entanglement links (green lines) between its qubits (black spheres) and a qubit in each neighboring node separately, via the transmission of photons through channels on the order of the attenuation length ($L/2$). Whichever link succeeds first (left hand is shown) is stored in memory until the remaining link succeeds. The maximum link attempt rate is inversely proportional to the photon travel time [$L/(2c)$]. (b) A Bell state measurement in the repeater node establishes entanglement between the neighboring nodes.

Specifically, photonic entanglement is established at the ends of two 25-km-long fiber channels with the repeater node in the middle. Next, the dominant cause of entanglement infidelity is identified and then the repeater node is shown to achieve a higher rate than when operated in a direct transmission configuration. Finally, in the future, the repeater node could be duplicated and concatenated to form repeater chains; the performance enhancements required for such chains to establish heralded, stored entanglement between ions 800 km apart are calculated.

Our trapped-ion quantum repeater node is presented in Fig. 2. The repeater node is based on two $^{40}Ca^{+}$ ions in a linear Paul trap and at the position of the waist of a near-concentric 20-mm-long Fabry-Perot optical cavity that achieves efficient photon collection [36,37] at 854 nm. Ions, 5.8 μm apart, are deterministically positioned at neighboring antinodes of a vacuum cavity mode [38]. Single photons are generated via a bichromatic cavity-mediated Raman transition [36,49], driven via a 393 nm Raman laser beam with a 1.2 μm waist at the ions. A Raman laser pulse on an ion in the state $|S\rangle$ (Fig. 2) ideally generates the maximally entangled state $(|D,H\rangle + |D',V\rangle)/\sqrt{2}$, where the first ket vector element describes the ion and the second describes two orthogonal polarizations of a photon emitted

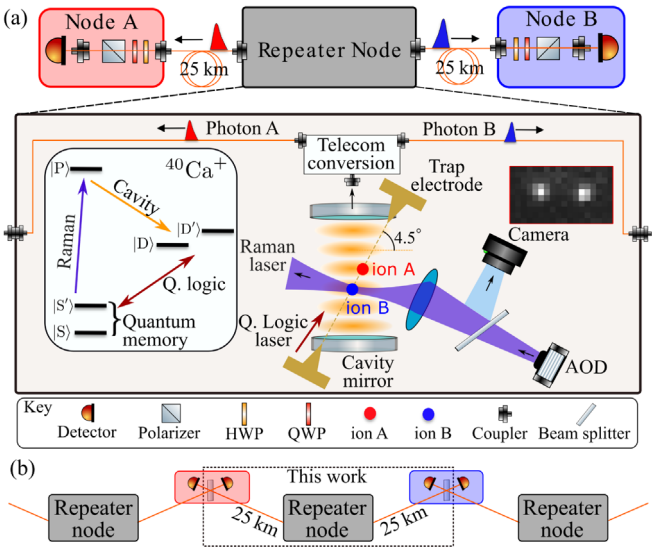

FIG. 2. Trapped-ion quantum repeater node. (a) Experimental schematic of an elementary network segment containing one repeater node. Photonic nodes A and B are each sent a telecom-converted [50,51] 1550 nm photon, entangled with a different ion, via 25-km-long fiber spools. Ion-qubit readout is done via imaging ion fluorescence at 397 nm on a camera. Ion-qubit quantum logic (Q. logic) gates are done via a 729 nm laser that couples equally to the ions. AOD, acousto-optic deflector; HWP, half-wave plate; QWP, quarter-wave plate. Level scheme: $|S\rangle = |4^2S_{1/2,m_j=-1/2}\rangle$, $|S'\rangle = |4^2S_{1/2,m_j=+1/2}\rangle$, $|P\rangle = |4^2P_{3/2,m_j=-3/2}\rangle$, $|D\rangle = |3^2D_{5/2,m_j=-5/2}\rangle$, $|D'\rangle = |3^2D_{5/2,m_j=-3/2}\rangle$. (b) Envisioned concatenation of the network segment in (a) into a repeater chain. Photon detection heralds remote ion entanglement [52].

into the cavity. After the photon has exited the cavity, the laser focus is moved to the cotrapped ion, allowing sequential generation of an ion-entangled photon from each ion. Each photon is converted to 1550 nm (telecom C band), via the system of Refs. [50,51]. Next, a fiber-coupled optical switch sends photons from ion A to photonic node A and photons from ion B to photonic node B [Fig. 2(a)], each via separate 25-km-long single-mode fiber spools.

The repeater protocol has four parts [38]: initialization, loop 1, loop 2, and DBSM (deterministic Bell state measurement), which are now summarized. Initialization prepares both ions in the state $|S\rangle$ and the ground state of the axial center-of-mass mode. Next, loop 1 begins, in which up to 29 attempts are made to distribute ion-entangled photons to both photonic nodes. Each loop-1 attempt includes two Raman pulses, one on each ion, followed by a 250 μs wait time: sufficient for a photon to travel over a 25 km fiber and, to simulate the remote nodes being 25 km away, for the "photon detected" signal to return. In the case of no detection events during all attempts in loop 1, the protocol is restarted. In the case of a photon detection event at *both* nodes during an attempt, loop 1 is aborted, a 729 nm laser pulse maps $|D'\rangle$ to $|S\rangle$ for both ions, and the DBSM is performed, as described below. In cases where either node A or B detects a photon during a loop-1 attempt, loop 1 is aborted, 729 nm laser pulses are applied to both ions, mapping $|D\rangle/|D'\rangle$ states to $|S\rangle/|S'\rangle$ states, respectively, and loop 2 begins. Those pulses transfer the qubit, encoded in the ion that generated the detected photon, into the $|S\rangle/|S'\rangle$ spin-qubit states, which serve as a quantum memory. In contrast to the $|D\rangle/|D'\rangle$ states, the spin-qubit states have no natural spontaneous decay rate, and suffer negligible differential ac Stark shifts imparted by single photons in the cavity or by laser light periodically injected into the cavity for length stabilization.

In loop 2, up to 190 attempts are made to distribute a photon, entangled with the ion not storing a qubit in memory, to the remaining remote node. Periodic spin echoes are executed to extend the memory coherence time: each flipping the $|S\rangle/|S'\rangle$ population using a sequence of 729 nm laser pulses. In cases where an attempt in loop 2 yields a photon detection event at the targeted remote node, both ion qubits are transferred into the states $|S\rangle$ and $|D\rangle$ and the DBSM is performed, otherwise the protocol is restarted.

Finally, the DBSM is performed in two steps [38]. First a laser-driven two-qubit Mølmer-Sorensen quantum logic gate [53–55] is applied. Second, the logical state of each ion qubit is measured via fluorescence state detection captured by a digital camera. Observing one of the four logical states of the ion qubits heralds the projection of the polarization of the remote telecom photons into one of four ideally orthogonal maximally entangled states. Those photonic states are characterized via quantum state tomography, done by repeating the protocol for a range of

polarization analysis settings at the photonic nodes. A fidelity over 0.5 between reconstructed and a maximally entangled states proves that the former is entangled [56].

The repeater protocol was executed 44 720 times over 33 min, during which 2229883 attempts were made to establish photonic entanglement between nodes A and B, and 2053 successes occurred (2049 during loop 2). The success probability is therefore $P_s = 9.2(2) \times 10^{-4}$. Successes correspond to asynchronous detection of a photon at each remote node, where each photon is detected within a 40-μs-wide time window containing the single-photon wave packets [Fig. 3(a)]. The value of P_s can be compared with the expected probability P_s^{single} to establish node A-B entanglement without exploiting the ion memories. We calculate $P_s^{\text{single}} = P_{A,1} \times P_{B,1} = 7.2(2) \times 10^{-6}$,

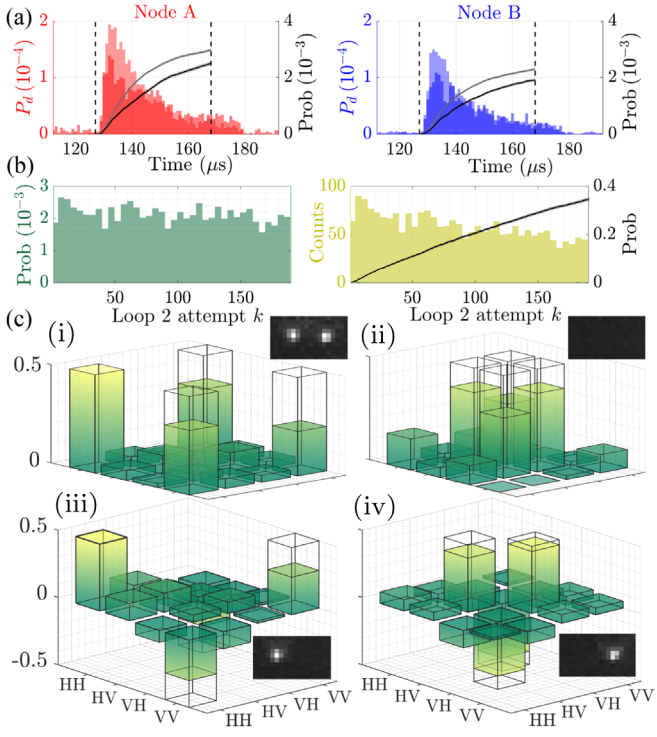

FIG. 3. Repeater protocol results. (a) Left axes: probability distribution (P_d) for single-photon detection per 1 μs time bin. Lighter and darker colored bars: loop 1 and loop 2 data, respectively. Time origins: Raman laser pulse onset. Dashed black lines: windows where DBSM is performed. Right axes: cumulative photon detection probability for loop 1 (lighter line) and loop 2 (darker line). (b) Photon detection probability (green bars) and counts (yellow bars) in attempt k of loop 2. Black line (right axis): cumulative photon detection (count) probability, totaling $P_2 = 0.346(4)$. (c) Colored bars show measured real parts of the density matrix of the two single-photon polarization qubits shared by nodes A and B, when ion B stored a qubit in memory. Fidelities with targeted Bell states (wire mesh) are (i) 72^{+7}_{-6}%, (ii) 67^{+7}_{-7}%, (iii) 69^{+6}_{-7}%, (iv) 0.83^{+6}_{-6}%. Absolute values of imaginary parts do not exceed 0.09. Inset camera images: corresponding two-ion measurement (DBSM) outcome.

where $P_{A,1} = 3.06(5) \times 10^{-3}$ and $P_{B,1} = 2.36(4) \times 10^{-3}$ are the measured probabilities for single-photon detection during a loop-1 attempt at nodes A and B, respectively. The memories thus enhance the success probability by a factor $\alpha = P_s/P_s^{\text{single}} = 128$. In principle, by performing enough loop-2 attempts, one can approach unit probability for the second photon detection ($P_2 = 1$) yielding the maximum memory enhancement factor for our experiment of $\alpha^{\max} = (P_{A,1} + P_{B,1})/(2P_s^{\text{single}}) = 375$. However, decoherence of the ion memories limits the number of loop-2 attempts before stored entanglement is lost. In the presented experiment, 190 attempts resulted in $P_2 = 0.346(4)$, limiting α to be $\alpha = \alpha^{\max} \times P_2$ [Fig. 3(b)].

Figure 3(c) presents the reconstructed two-photon density matrices in the cases when ion B stored a qubit in memory. Each matrix has been rotated, from the one directly reconstructed, by the same two single-qubit rotations. Those local rotations, found by numerical search to maximize the average fidelities with Bell states, do not change the entanglement content of the four states, nor their inner product, and bring the measured states into the familiar Bell state form. The Bell state fidelities of the measured states are $[72^{+7}_{-6}, 67^{+7}_{-7}, 69^{+6}_{-7}, 83^{+6}_{-6}]$%.

Consequently, a different set of local rotations is used to rotate the states into the Bell form when ion A stored a qubit in memory, yielding fidelities of $[63^{+7}_{-8}, 67^{+7}_{-7}, 59^{+7}_{-8}, 77^{+7}_{-7}]$% with the corresponding Bell states. Using the data underlying all eight states, a numerical calculation is performed to simulate the process known as feed forward, in which the photon states are further locally rotated such that the repeater always delivers a single Bell state to the remote nodes: A fidelity of 72^{+2}_{-2}% is obtained [38].

To identify origins of protocol infidelity, the ion-photon states stored in memory are characterized in a separate experiment. Here, a modified repeater protocol is performed: up to 30 loop 1 attempts are made to detect a photon from ion A only. In successful cases, ion-qubit A is stored in memory while a fixed number of loop 2 attempts k are made to generate a photon from ion B. Finally, state tomography of the joint state of ion-qubit A and the detected photonic qubit "a" $[\rho_{Aa}(k)]$ is performed. That experiment is performed without fiber spools and telecom conversion for improved efficiencies, but wait times are retained allowing for twice 25 km of photon travel. Figure 4 shows how the fidelity of the measured $\rho_{Aa}(k)$ states, with respect to the maximally entangled state nearest to $\rho_{Aa}(0)$, evolves. The initial fidelity of 0.96(2) drops to 0.64(2) after 195 attempts, corresponding to a memory storage time of $t = 64$ ms. The dynamics are modeled with a single-qubit map that realizes ion-qubit memory dephasing with a Gaussian temporal profile parametrized by a decoherence time τ [38]. Applying the map to the initial state $\rho_{Aa}(0)$ yields modeled time-evolved states $\tilde{\rho}_{Aa}(t, \tau)$, which have

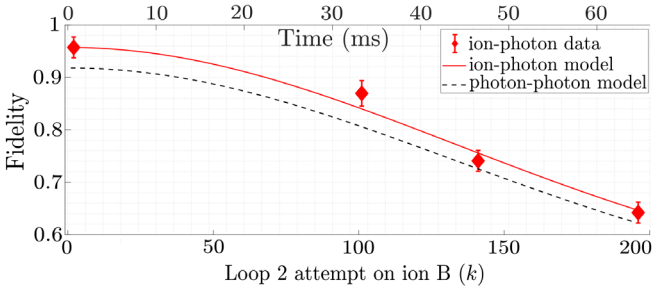

FIG. 4. Quantum memory performance. Red diamonds: fidelity between the ion-photon state stored in ion A after k photon generation attempts on neighboring ion B, $\rho_{Aa}(k)$, and the maximally entangled state closest to $\rho_{Aa}(0)$. Red line: fit of the fidelity of the modeled ion-photon state (see text) stored in ion A, $\tilde{\rho}_{Aa}(t)$, to the data, yielding an ion-qubit decoherence time of $\tau = 62(3)$ ms. Black dashed line: Bell state fidelity of the modeled photon-photon state established in attempt k, using perfect DBSM and feed forward (see text). Time axis: average attempt duration. Error bars represent one standard deviation of uncertainty due to Poissonian photon counting statistics.

fidelities $F[\tilde{\rho}_{Aa}(t,\tau)]$ with respect to the nearest maximally entangled state to $\rho_{Aa}(0)$. A fit of the model to the data yields $\tau = 62 \pm 3$ ms (solid red line, Fig. 4). The model is now extended to predict the two-photon states reconstructed in the full repeater protocol [38]. Here, for the ion-photon states stored in memory, the states $\tilde{\rho}_{Aa}(t, \tau = 62\,\mathrm{ms})$ are used for both ions. For the ion-photon states not stored in memory, the state $\rho_A(0)$ is used for both ions. All other parts of the repeater protocol, and feed forward, are modeled without imperfection. The predicted two-photon Bell state fidelities, established between the remote nodes at step k of loop 2, are plotted as a dashed black line in Fig. 4. Finally, the modeled two-photon states at each attempt (k) are added up as a mixture, weighted by the probability with which they occurred in the repeater experiment [Fig. 3(b)], yielding a predicted photonic Bell state fidelity for the repeater protocol of 0.813(7). Considering the experimentally obtained value of 72(2)%, we conclude that our model captures the dominant sources of infidelity in the repeater protocol: decoherence of the ion memories.

The results of an independent experimental investigation into the origins of the ion-memory decoherence [38] are now summarized. Raman laser pulses on the neighboring ion during the repeater protocol decrease the ion-memory coherence time from $\tau = 108(1)$ to 59(1) ms. A significant contribution to this decrease is made by imperfections in the spin echoes caused by the initial and increasing temperature of ion string. The heating is caused by the ion in the Raman laser focus absorbing and spontaneously emitting 393 nm photons. No significant direct interactions between an ion's memory qubit and Raman laser pulses on the neighboring ion were found.

In our last experiment, performance in repeater configuration is compared with that in a direct transmission configuration. For direct transmission, the fiber spools are joined into a 50 km channel. Furthermore, only the initialization and loop 1 of the repeater protocol are executed, both ion-entangled photons are directed to node B, and the detection of any one photon counts as a success. The wait time after photon generation is set to 500 μs to allow for twice the 50 km travel time. In both configurations, attempt rates are predominantly limited by the photon travel and signal return times, and polarization analysis is removed to improve overall efficiency. Having previously observed maximal ion-photon entanglement over 50 km with a fidelity of 0.86 ± 0.03 in direct configuration with a single ion [50], we focus here on measuring the success rates. The results are absolute success rates of 5.9 and 3.8 Hz for the repeater and direct transmission configurations, respectively. After excluding slight differences in initialization and dead times [38], we obtain success rates of 9.2 and 6.7 Hz, where the repeater is still faster. Analytic expressions for the performance requirements for a repeater node to beat itself in direct transmission are summarized in Ref. [38].

We now present parameter combinations for future enhanced versions of our repeater nodes that would enable a significant advance in the state of the art for entanglement distribution between remote matter [16]. We consider the repeater node chains [Fig. 2(b)] and model of Ref. [33] to calculate the average time (T_{tot}) to establish heralded entanglement between one ion in each end node. The key model parameter is $P^0_{\mathrm{link}} = 0.21$: the combined telecom photon generation and detection probability for each node excluding channel (fiber) losses. For a two-node chain with a 50 km telecom fiber between them, one obtains $T_{\mathrm{tot}} = 0.07$ s. For a 17 node chain across 800 km of telecom fiber, one obtains $T_{\mathrm{tot}} = 0.7$ s. Despite the channel loss probability increasing by 13 orders of magnitude (50 to 800 km), and commensurate rate reduction for direct transmission schemes, the repeater-assisted entanglement distribution rate is predicted to drop by only a factor of 10.

We introduce a simple model for the established Bell state fidelity across the 800 km chain [38]. The model does not consider memory decoherence, which is valid under the condition that the memory coherence time in each node is much longer than the average entanglement distribution time between the end nodes, that is $\tau \gg 0.7$ s. The model parameters are F_0, the ion-photon Bell state fidelity; $F^{\mathrm{ions}}_{\mathrm{swap}}$, the DBSM fidelity; and $F^{\mathrm{photon}}_{\mathrm{swap}}$, a nondeterministic photonic Bell state measurement fidelity. When all three fidelities are 0.99, the model predicts a Bell state fidelity of 0.61, which is over the 0.5 threshold.

The required enhanced ion-node parameters are ambitious but feasible. The current repeater node achieves [$P^0_{\mathrm{link}} = 0.018(1)$, $\tau = 62(3)$ ms, $F_0 = 0.96(2)$, $F^{\mathrm{ions}}_{\mathrm{swap}} = 0.95(2)$, $F^{\mathrm{photon}}_{\mathrm{swap}} = 0.69(2)$], where the last value is taken

from the two-photon interference contrast at telecom wavelengths measured in Ref. [57]. The required improvements in F_0 and $F_{\mathrm{swap}}^{\mathrm{ions}}$ are minor, while those in P_{link}^{0} may already be possible by combining the single ion-photon collection efficiencies of Ref. [36] and the telecom conversion efficiency of Ref. [58]. Memory times of tens of seconds in the repeater node should be possible by combining decoherence-free subspaces [59,60] with sympathetic cooling [61,62] or directly using other isotopes [63]. Achieving the required $F_{\mathrm{swap}}^{\mathrm{photon}}$, while maintaining $P_{\mathrm{link}}^{0} = 0.21$, may be achieved by combing the methods of Refs. [36,64] with a smaller mode-volume cavity and careful attention to minimize birefringence [65].

A long-distance quantum repeater node based on trapped ions with an optical cavity was demonstrated, as envisioned in Ref. [33]. Two remote trapped ions have previously been entangled over a few meters [11,14,22,23] and, using the ion-cavity system of this work, over 230 m [24]. The results in this work, in combination with those in Refs. [24,57], demonstrate all key capabilities of a long-distance quantum repeater platform in a single system. In the future, more qubits could be directly integrated into the node [33] allowing for quantum error correction and multimoding [6].

Datasets available [66].

This work was financially supported by the START prize of the Austrian FWF project Y 849-N20, the Austrian FWF Standalone project QMAP Project No. P 34055, the Institute for Quantum Optics and Quantum Information (IQOQI) of the Austrian Academy Of Sciences (OeAW), and the European Union's Horizon 2020 research and innovation program under Grant Agreement No. 820445 and project name "Quantum Internet Alliance." We acknowledge funding for V. K. by the Erwin Schrödinger Center for Quantum Science & Technology (ESQ) Discovery Programme, for N. S. by the Commissariat à l'Energie Atomique et aux Energies Alternatives (CEA), and for B. P. L. by the CIFAR Quantum Information Science Program of Canada. Experimental data taking was done by V. K., M. M., V. K., and M. C. Development of the experimental setup was done by V. K., M. C., M. M, J. B., J. S., and B. P. L. Data analysis and interpretation was done by V. K., M. C., M. M., J. B., and B. P. L. Modeling was done by V. K., J. B., M. C., and N. S. The manuscript was written by B. P. L. and V. K., with all authors providing detailed comments. The project was conceived and supervised by B. P. L.

*Corresponding author.
ben.lanyon@uibk.ac.at

[1] H. J. Kimble, The quantum internet, Nature (London) **453**, 1023 (2008).
[2] S. Wehner, D. Elkouss, and R. Hanson, Quantum internet: A vision for the road ahead, Science **362** (2018).
[3] H.-J. Briegel, W. Dür, J. I. Cirac, and P. Zoller, Quantum Repeaters: The Role of Imperfect Local Operations in Quantum Communication, Phys. Rev. Lett. **81**, 5932 (1998).
[4] L.-M. Duan, M. D. Lukin, J. I. Cirac, and P. Zoller, Long-distance quantum communication with atomic ensembles and linear optics, Nature (London) **414**, 413 (2001).
[5] N. Sangouard, C. Simon, H. de Riedmatten, and N. Gisin, Quantum repeaters based on atomic ensembles and linear optics, Rev. Mod. Phys. **83**, 33 (2011).
[6] C. Simon, H. de Riedmatten, M. Afzelius, N. Sangouard, H. Zbinden, and N. Gisin, Quantum Repeaters with Photon Pair Sources and Multimode Memories, Phys. Rev. Lett. **98**, 190503 (2007).
[7] L. Jiang, J. M. Taylor, K. Nemoto, W. J. Munro, R. Van Meter, and M. D. Lukin, Quantum repeater with encoding, Phys. Rev. A **79**, 032325 (2009).
[8] K. Azuma, K. Tamaki, and H.-K. Lo, All-photonic quantum repeaters, Nat. Commun. **6**, 6787 (2015).
[9] W. J. Munro, K. Azuma, K. Tamaki, and K. Nemoto, Inside quantum repeaters, IEEE J. Sel. Top. Quantum Electron. **21**, 78 (2015).
[10] G. Avis, F. F. da Silva, T. Coopmans, A. Dahlberg, H. Jirovská, D. Maier, J. Rabbie, A. Torres-Knoop, and S. Wehner, Requirements for a processing-node quantum repeater on a real-world fiber grid, arXiv:2207.10579.
[11] D. L. Moehring, P. Maunz, S. Olmschenk, K. C. Younge, D. N. Matsukevich, L.-M. Duan, and C. Monroe, Entanglement of single-atom quantum bits at a distance, Nature (London) **449**, 68 (2007).
[12] S. Ritter, C. Nölleke, C. Hahn, A. Reiserer, A. Neuzner, M. Uphoff, M. Mücke, E. Figueroa, J. Bochmann, and G. Rempe, An elementary quantum network of single atoms in optical cavities, Nature (London) **484**, 195 (2012).
[13] B. Hensen, H. Bernien, A. E. Dréau, A. Reiserer, N. Kalb, M. S. Blok, J. Ruitenberg, R. F. L. Vermeulen, R. N. Schouten, C. Abellán, W. Amaya, V. Pruneri, M. W. Mitchell, M. Markham, D. J. Twitchen, D. Elkouss, S. Wehner, T. H. Taminiau, and R. Hanson, Loophole-free Bell inequality violation using electron spins separated by 1.3 kilometres, Nature (London) **526**, 682 (2015).
[14] L. J. Stephenson, D. P. Nadlinger, B. C. Nichol, S. An, P. Drmota, T. G. Ballance, K. Thirumalai, J. F. Goodwin, D. M. Lucas, and C. J. Ballance, High-Rate, High-Fidelity Entanglement of Qubits Across an Elementary Quantum Network, Phys. Rev. Lett. **124**, 110501 (2020).
[15] M. Pompili, S. L. N. Hermans, S. Baier, H. K. C. Beukers, P. C. Humphreys, R. N. Schouten, R. F. L. Vermeulen, M. J. Tiggelman, L. dos Santos Martins, B. Dirkse, S. Wehner, and R. Hanson, Realization of a multinode quantum network of remote solid-state qubits, Science **372**, 259 (2021).
[16] T. van Leent, M. Bock, F. Fertig, R. Garthoff, S. Eppelt, Y. Zhou, P. Malik, M. Seubert, T. Bauer, W. Rosenfeld, W. Zhang, C. Becher, and H. Weinfurter, Entangling single atoms over 33 km telecom fibre, Nature (London) **607**, 69 (2022).
[17] J. Hofmann, M. Krug, N. Ortegel, L. Gérard, M. Weber, W. Rosenfeld, and H. Weinfurter, Heralded entanglement between widely separated atoms, Science **337**, 72 (2012).
[18] H. Bernien, B. Hensen, W. Pfaff, G. Koolstra, M. S. Blok, L. Robledo, T. H. Taminiau, M. Markham, D. J. Twitchen,

L. Childress, and R. Hanson, Heralded entanglement between solid-state qubits separated by three metres, Nature (London) **497**, 86 (2013).
[19] A. Delteil, Z. Sun, W.-b. Gao, E. Togan, S. Faelt, and A. Imamoğlu, Generation of heralded entanglement between distant hole spins, Nat. Phys. **12**, 218 (2016).
[20] R. Stockill, M. J. Stanley, L. Huthmacher, E. Clarke, M. Hugues, A. J. Miller, C. Matthiesen, C. Le Gall, and M. Atatüre, Phase-Tuned Entangled State Generation between Distant Spin Qubits, Phys. Rev. Lett. **119**, 010503 (2017).
[21] P. Magnard, S. Storz, P. Kurpiers, J. Schär, F. Marxer, J. Lütolf, T. Walter, J.-C. Besse, M. Gabureac, K. Reuer, A. Akin, B. Royer, A. Blais, and A. Wallraff, Microwave Quantum Link between Superconducting Circuits Housed in Spatially Separated Cryogenic Systems, Phys. Rev. Lett. **125**, 260502 (2020).
[22] L.-M. Duan and C. Monroe, Colloquium: Quantum networks with trapped ions, Rev. Mod. Phys. **82**, 1209 (2010).
[23] B. C. Nichol, R. Srinivas, D. P. Nadlinger, P. Drmota, D. Main, G. Araneda, C. J. Ballance, and D. M. Lucas, An elementary quantum network of entangled optical atomic clocks, Nature (London) **609**, 689 (2022).
[24] V. Krutyanskiy, M. Galli, V. Krcmarsky, S. Baier, D. A. Fioretto, Y. Pu, A. Mazloom, P. Sekatski, M. Canteri, M. Teller, J. Schupp, J. Bate, M. Meraner, N. Sangouard, B. P. Lanyon, and T. E. Northup, Entanglement of Trapped-Ion Qubits Separated by 230 Meters, Phys. Rev. Lett. **130**, 050803 (2023).
[25] F. Bussières, C. Clausen, A. Tiranov, B. Korzh, V. B. Verma, S. W. Nam, F. Marsili, A. Ferrier, P. Goldner, H. Herrmann, C. Silberhorn, W. Sohler, M. Afzelius, and N. Gisin, Quantum teleportation from a telecom-wavelength photon to a solid-state quantum memory, Nat. Photonics **8**, 775 (2014).
[26] W. Chang, C. Li, Y.-K. Wu, N. Jiang, S. Zhang, Y.-F. Pu, X.-Y. Chang, and L.-M. Duan, Long-Distance Entanglement between a Multiplexed Quantum Memory and a Telecom Photon, Phys. Rev. X **9**, 041033 (2019).
[27] D. Lago-Rivera, S. Grandi, J. V. Rakonjac, A. Seri, and H. de Riedmatten, Telecom-heralded entanglement between multimode solid-state quantum memories, Nature (London) **594**, 37 (2021).
[28] S. Langenfeld, P. Thomas, O. Morin, and G. Rempe, Quantum Repeater Node Demonstrating Unconditionally Secure Key Distribution, Phys. Rev. Lett. **126**, 230506 (2021).
[29] C.-W. Chou, J. Laurat, H. Deng, K. S. Choi, H. de Riedmatten, D. Felinto, and H. J. Kimble, Functional quantum nodes for entanglement distribution over scalable quantum networks, Science **316**, 1316 (2007).
[30] Y.-F. Pu, S. Zhang, Y.-K. Wu, N. Jiang, W. Chang, C. Li, and L.-M. Duan, Experimental demonstration of memory-enhanced scaling for entanglement connection of quantum repeater segments, Nat. Photonics **15**, 374 (2021).
[31] P. C. Humphreys, N. Kalb, J. P. J. Morits, R. N. Schouten, R. F. L. Vermeulen, D. J. Twitchen, M. Markham, and R. Hanson, Deterministic delivery of remote entanglement on a quantum network, Nature (London) **558**, 268 (2018).
[32] M. K. Bhaskar, R. Riedinger, B. Machielse, D. S. Levonian, C. T. Nguyen, E. N. Knall, H. Park, D. Englund, M. Lončar, D. D. Sukachev, and M. D. Lukin, Experimental demonstration of memory-enhanced quantum communication, Nature (London) **580**, 60 (2020).
[33] N. Sangouard, R. Dubessy, and C. Simon, Quantum repeaters based on single trapped ions, Phys. Rev. A **79**, 042340 (2009).
[34] N. Kalb, A. A. Reiserer, P. C. Humphreys, J. J. W. Bakermans, S. J. Kamerling, N. H. Nickerson, S. C. Benjamin, D. J. Twitchen, M. Markham, and R. Hanson, Entanglement distillation between solid-state quantum network nodes, Science **356**, 928 (2017).
[35] S. L. N. Hermans, M. Pompili, H. K. C. Beukers, S. Baier, J. Borregaard, and R. Hanson, Qubit teleportation between non-neighbouring nodes in a quantum network, Nature (London) **605**, 663 (2022).
[36] J. Schupp, V. Krcmarsky, V. Krutyanskiy, M. Meraner, T. E. Northup, and B. P. Lanyon, Interface between trapped-ion qubits and traveling photons with close-to-optimal efficiency, PRX Quantum **2**, 020331 (2021).
[37] J. Schupp, Interface between trapped-ion qubits and travelling photons with close-to-optimal efficiency, Ph.D. thesis, University of Innsbruck, 2021.
[38] See Supplemental Material at http://link.aps.org/supplemental/10.1103/PhysRevLett.130.213601, which includes Refs. [39–48], for details on the experimental setup layout and sequence, entangled states reconstruction including unitary rotations, investigation, and modeling of the ion-memory decoherence, and modeling of the future systems.
[39] M. Lee, K. Friebe, D. A. Fioretto, K. Schüppert, F. R. Ong, D. Plankensteiner, V. Torggler, H. Ritsch, R. Blatt, and T. E. Northup, Ion-Based Quantum Sensor for Optical Cavity Photon Numbers, Phys. Rev. Lett. **122**, 153603 (2019).
[40] M. Canteri, Single-atom-focused laser for photon generation and qubit control, Master's thesis, University of Innsbruck, 2020.
[41] G. Kirchmair, Quantum non-demolition measurements and quantum simulation, Ph.D. thesis, University of Innsbruck, 2010.
[42] M. Ježek, J. Fiurášek, and Z. c. v. Hradil, Quantum inference of states and processes, Phys. Rev. A **68**, 012305 (2003).
[43] S. A. Hill and W. K. Wootters, Entanglement of a Pair of Quantum Bits, Phys. Rev. Lett. **78**, 5022 (1997).
[44] S. Pirandola, R. Laurenza, C. Ottaviani, and L. Banchi, Fundamental limits of repeaterless quantum communications, Nat. Commun. **8**, 15043 (2017).
[45] V. Scarani, H. Bechmann-Pasquinucci, N. J. Cerf, M. Dušek, N. Lütkenhaus, and M. Peev, The security of practical quantum key distribution, Rev. Mod. Phys. **81**, 1301 (2009).
[46] P. van Loock, W. Alt, C. Becher, O. Benson, H. Boche, C. Deppe, J. Eschner, S. Höfling, D. Meschede, P. Michler, F. Schmidt, and H. Weinfurter, Extending quantum links: Modules for fiber- and memory-based quantum repeaters, Adv. Quantum Technol. **3**, 1900141 (2020).
[47] F. Rozpedek, R. Yehia, K. Goodenough, M. Ruf, P. C. Humphreys, R. Hanson, S. Wehner, and D. Elkouss, Near-term quantum-repeater experiments with nitrogen-vacancy centers: Overcoming the limitations of direct transmission, Phys. Rev. A **99**, 052330 (2019).

[48] A. N. Craddock, J. Hannegan, D. P. Ornelas-Huerta, J. D. Siverns, A. J. Hachtel, E. A. Goldschmidt, J. V. Porto, Q. Quraishi, and S. L. Rolston, Quantum Interference between Photons from an Atomic Ensemble and a Remote Atomic Ion, Phys. Rev. Lett. **123**, 213601 (2019).

[49] A. Stute, B. Casabone, P. Schindler, T. Monz, P. O. Schmidt, B. Brandstätter, T. E. Northup, and R. Blatt, Tunable ion-photon entanglement in an optical cavity, Nature (London) **485**, 482 (2012).

[50] V. Krutyanskiy, M. Meraner, J. Schupp, V. Krcmarsky, H. Hainzer, and B. P. Lanyon, Light-matter entanglement over 50 km of optical fibre, npj Quantum Inf. **5**, 72 (2019).

[51] V. Krutyanskiy, M. Meraner, J. Schupp, and B. P. Lanyon, Polarisation-preserving photon frequency conversion from a trapped-ion-compatible wavelength to the telecom C-band, Appl. Phys. B **123**, 228 (2017).

[52] L. Luo, D. Hayes, T. A. Manning, D. N. Matsukevich, P. Maunz, S. Olmschenk, J. D. Sterk, and C. Monroe, Protocols and techniques for a scalable atom-photon quantum network, Fortschr. Phys. **57**, 1133 (2009).

[53] A. Sørensen and K. Mølmer, Quantum Computation with Ions in Thermal Motion, Phys. Rev. Lett. **82**, 1971 (1999).

[54] A. Sørensen and K. Mølmer, Entanglement and quantum computation with ions in thermal motion, Phys. Rev. A **62**, 022311 (2000).

[55] J. Benhelm, G. Kirchmair, C. F. Roos, and R. Blatt, Towards fault-tolerant quantum computing with trapped ions, Nat. Phys. **4**, 463 (2008).

[56] C. A. Sackett, D. Kielpinski, B. E. King, C. Langer, V. Meyer, C. J. Myatt, M. Rowe, Q. A. Turchette, W. M. Itano, D. J. Wineland, and C. Monroe, Experimental entanglement of four particles, Nature (London) **404**, 256 (2000).

[57] M. Meraner, A. Mazloom, V. Krutyanskiy, V. Krcmarsky, J. Schupp, D. A. Fioretto, P. Sekatski, T. E. Northup, N. Sangouard, and B. P. Lanyon, Indistinguishable photons from a trapped-ion quantum network node, Phys. Rev. A **102**, 052614 (2020).

[58] M. Bock, Polarization-preserving quantum frequency conversion for trapped-atom based quantum networks, Ph.D. thesis, University of Saarbrucken, 2020.

[59] M. Zwerger, B. P. Lanyon, T. E. Northup, C. A. Muschik, W. Dür, and N. Sangouard, Quantum repeaters based on trapped ions with decoherence-free subspace encoding, Quantum Sci. Technol. **2**, 044001 (2017).

[60] H. Häffner, F. Schmidt-Kaler, W. Hänsel, C. F. Roos, T. Körber, M. Chwalla, M. Riebe, J. Benhelm, U. D. Rapol, C. Becher, and R. Blatt, Robust entanglement, Appl. Phys. B **81**, 151 (2005).

[61] T. Rosenband, P. O. Schmidt, D. B. Hume, W. M. Itano, T. M. Fortier, J. E. Stalnaker, K. Kim, S. A. Diddams, J. C. J. Koelemeij, J. C. Bergquist, and D. J. Wineland, Observation of the $^1s_0 \rightarrow {}^3p_0$ Clock Transition in $^{27}Al^+$, Phys. Rev. Lett. **98**, 220801 (2007).

[62] J. P. Home, M. J. McDonnell, D. J. Szwer, B. C. Keitch, D. M. Lucas, D. N. Stacey, and A. M. Steane, Memory coherence of a sympathetically cooled trapped-ion qubit, Phys. Rev. A **79**, 050305(R) (2009).

[63] P. Drmota, D. Main, D. P. Nadlinger, B. C. Nichol, M. A. Weber, E. M. Ainley, A. Agrawal, R. Srinivas, G. Araneda, C. J. Ballance, and D. M. Lucas, Robust Quantum Memory in a Trapped-Ion Quantum Network Node, Phys. Rev. Lett. **130**, 090803 (2022).

[64] T. Walker, S. V. Kashanian, T. Ward, and M. Keller, Improving the indistinguishability of single photons from an ion-cavity system, Phys. Rev. A **102**, 032616 (2020).

[65] E. Kassa, W. J. Hughes, S. Gao, and J. F. Goodwin, Effects of cavity birefringence in polarisation-encoded quantum networks, New J. Phys. **25**, 013004 (2023).

[66] V. Krutyanskiy, M. Canteri, M. Meraner, J. Bate, V. Krcmarsky, J. Schupp, N. Sangouard, and B. P. Lanyon, A telecom-wavelength quantum repeater node based on a trapped-ion processor (2023), 10.5281/zenodo.7781415.